01 Oct 2022

Characterizing and Modeling the Coupled Hydro-Mechanical Cyclic Behavior of Unsaturated Soils using Constant Water Content Oedometer and Direct Shear Tests

Beshoy Riad

Xiong Zhang
Missouri University of Science and Technology, zhangxi@mst.edu

Recommended Citation

B. Riad and X. Zhang, "Characterizing and Modeling the Coupled Hydro-Mechanical Cyclic Behavior of Unsaturated Soils using Constant Water Content Oedometer and Direct Shear Tests," *Transportation Research Record*, vol. 2676, no. 10, pp. 173 - 193, SAGE Publications, Oct 2022.
The definitive version is available at https://doi.org/10.1177/03611981221088775

TRR
JOURNAL OF THE TRANSPORTATION RESEARCH BOARD

Research Article

Transportation Research Record
2022, Vol. 2676(10) 173–193

DOI: 10.1177/03611981221088775
journals.sagepub.com/home/trr
SAGE

Characterizing and Modeling the Coupled Hydro-Mechanical Cyclic Behavior of Unsaturated Soils Using Constant Water Content Oedometer and Direct Shear Tests

Beshoy Riad[1] and Xiong Zhang[1]

Abstract

Most transportation infrastructures are constructed on compacted soils that are typically unsaturated above the groundwater table. The soils are subjected to cyclic traffic loadings and seasonal wetting–drying cycles. Although problems associated with unsaturated soils are ubiquitous in the US, coupled hydro-mechanical analysis is rarely included in the design/analysis of transportation geosystems. This can be attributed to two main reasons: (a) there are no simple devices/methods which can be used to rapidly characterize stress–strain behavior for unsaturated soils, and (b) there is a lack of a constitutive model to study coupled hydro-mechanical cyclic behavior for unsaturated soils in a consistent way. This paper takes advantage of the recent advancements in suction measurement and constitutive modeling to overcome these limitations. In this paper, conventional oedometer and direct shear tests for saturated soils are modified to characterize stress–strain behavior of unsaturated soils under cyclic undrained loading conditions. Then, series of constant water content cyclic oedometer and direct shear tests are performed to characterize the hydro-mechanical behavior of a silty soil. Moreover, methods are developed to use results from both tests to calibrate parameters for a recently proposed hydro-mechanical constitutive model. The paper also compares the model predictions with the measured results. Results indicate that the model is able to satisfactorily predict the hydro-mechanical hysteresis behavior of the soil. With developments in equipment, constitutive models, and analysis, it is now possible to fully characterize the hydro-mechanical behavior of unsaturated soils in a more efficient manner.

Keywords

infrastructure, geology and geoenvironmental engineering, mechanics and drainage of saturated and unsaturated geomaterials, partially saturated soils, constitutive modeling, and cyclic hydro-mechanical behavior

Unsaturated soils are often involved in many engineering problems of practical interest. In transportation applications, for instance, soils are typically subjected to cycles of loading and unloading (i.e., traffic loads) or wetting–drying (i.e., rainfall and droughts). Plastic strains may be cumulated as a result of repeated mechanical and hydraulic loading cycles. Consequently, roads are suffering from deteriorations, rutting, and, sometimes, failures (*1, 2*). To properly solve such problems, it is necessary to develop a good understanding of the unsaturated soil behavior by means of understanding the interaction between different soil phases (i.e., liquid, gas, and solid). Two essential elements are needed to develop such a good understanding: (a) unsaturated soil characterization and (b) soil behavior modeling.

In respect of soil characterization, Bishop and Donald (*3*) developed the first suction-controlled triaxial (SCTX) testing apparatus, and now it has been a standard for the characterization of stress–strain behavior for unsaturated soils (*4–6*). However, the apparatus is very sophisticated

[1]Department of Civil, Architectural, and Environmental Engineering, Missouri University of Science and Technology, Rolla, MO

Corresponding Author:
Xiong Zhang, zhangxi@mst.edu

and expensive ($100,000 each). In addition, the SCTX test is a consolidated drained test. Thus, it is very time-consuming to perform a test as a result of the low permeability of unsaturated soils. It often takes 3 to 4 years to fully characterize one unsaturated soil (*7–9*).

Moreover, numerous efforts have been dedicated to modifying the conventional oedometer and direct shear devices to use them for unsaturated soils. For shear strength characterization, researchers developed and used the suction-controlled direct shear test, in which soil suction was controlled using the axis-translation technique (*10–13*). Similarly, for stiffness characterization, researchers modified the oedometer test by introducing a suction control system through axis-translation or vapor equilibrium technique (*14–18*). These devices, however, have suffered from several limitations. They often require the implementation of major modifications into the conventional saturated soil testing devices. Moreover, they require suction control (i.e., drained conditions). Because of the extremely low permeability of unsaturated soils, testing time is too long. For the oedometer test, because of the unknown stress path, there was no method available to use its results for constitutive modeling. However, Zhang et al. (*19*) derived an explicit formulation for the at-rest earth pressure coefficient (K_0). Therefore, they were able to calculate the lateral stress during oedometer testing and, consequently, the stress path is known. Accordingly, they develop a method to take advantage of the oedometer test results for constitutive modeling purposes. However, oedometer tests are non-failure tests. Thus, the strength parameters, calibrated in Zhang et al. (*19*), are extrapolation for the soil behavior, and may be subject to significant errors.

Tensiometers have been used in the geoscience field for decades. However, the measurement capacity for a conventional tensiometer was limited to 100 kPa because of water cavitation (*20*). Ridley and Burland (*21*) developed the first high-suction tensiometer (HST) with a capacity of 1500 kPa. Since then, many HSTs have been developed and successfully used in field and laboratory testing (*22–30*). Reviews of the latest developments in HSTs and their applications can be found in (*30–32*). Many researchers have used the HST for determining the soil–water characteristic curve (*33–40*). Moreover, the HST was used in many applications for measuring suction changes during mechanical and hydraulic loading. For instance, HSTs were used for unconfined compression testing (*41, 42*), oedometer testing (*43*), and triaxial testing (*26, 44, 45*).

In respect of soil modeling, Alonso et al. (*46*) proposed the first elastoplastic model for unsaturated soils. The model gained considerable acceptance and has been implemented into numerical schemes. The model was later named the Barcelona Basic Model (BBM). However, an inconsistency between the hydraulic and mechanical behaviors was noticed by Wheeler and Karube (*47*). It was mainly related to using a simple elastic equation to represent the hydraulic behavior that is considered inconsistent with the elastoplastic mechanical behavior. Later, several modifications were proposed aiming at improving the shear and isotropic behaviors in the original BBM (*48, 49*). These models, however, focused on mechanical behavior only.

To better represent the hydraulic behavior, Wheeler (*50*) proposed two specific water volume surface equations to represent the hydraulic behavior. However, the macro-void changes were assumed to be fully plastic. Consequently, inconsistent predictions were noticed for the elastic and plastic hydraulic behaviors. Then, Vaunat et al. (*51*) proposed the first coupled hydro-mechanical constitutive model for unsaturated soils with a focus on hydraulic hysteresis, while the mechanical behavior was simulated using the BBM. However, an inconsistency was noticed because of the coupling effects between the hydraulic and mechanical behaviors of unsaturated soils. A review of the most common constitutive models for unsaturated soils can be found in Wheeler and Karube (*47*), Gens et al. (*52*), Gens (*53*), Jommi (*54*), and Zhang et al. (*55*). All the models mentioned above adopted the suction and net stress as independent stress state variables.

Other models were proposed considering the effective stress principles (*56–65*). Among these models, the model proposed by Wheeler et al. (*56*) was extended to anisotropic stress conditions and referred to as the Glasgow Coupled Model (GCM) (*65*). However, Raveendiraraj (*66*) noticed that the model predicted a non-unique saturated normal compression line, which caused non-smooth transition between the saturated and unsaturated soil states. In addition, the stress state variables used in the model incorporate the strain variables (i.e., porosity, n and degree of saturation, S_r). This caused difficulties in running quantitative predictions. Sheng et al. (*67*) proposed a model using a different pair of stress state variables. The model was then named SFG after the authors names (i.e., Sheng, Fredlund, and Gens). However, Zhang and Lytton (*68*) noticed an inconsistency between volumetric and hydraulic behaviors in the model and other issues that violated the theory of elastoplasticity.

Zhang and Lytton (*69, 70*) proposed a modified state surface approach (MSSA) to study the volume change for unsaturated soils. Later, the MSSA was extended to study the coupled hydro-mechanical behavior of unsaturated soils (*71*). Special attention was paid to the compatibility among the elastoplastic relations for the three soil phases (i.e., soil solids, water, and air). Representing the undrained soil behavior in a consistent manner was a challenge to most existing models. This challenge was addressed and solved by the coupled MSSA (*71*). The

coupled MSSA was then used successfully to predict the soil behavior, for different soils, under drained and undrained conditions (*41, 43, 71, 72*). The original MSSA (*69–71*) was based on critical state soil mechanics in which the soil hysteresis behavior was neglected. Recently, Riad and Zhang (*73*) extended the MSSA to account for coupled hydro-mechanical behavior considering both hydraulic and mechanical hysteresis. It is worth noting that mechanical hysteresis is neglected by most of the existing models.

Moreover, Riad and Zhang (*74*) further extended the MSSA to predict the soil behavior under general stress conditions and accordingly proposed a new model. The model can predict many unsaturated soils' behavioral features such as (a) elastoplastic behavior, (b) coupled hydro-mechanical behavior under isotropic and triaxial stress conditions, (c) both mechanical and hydraulic hysteresis; in addition, it (d) has a smooth transition between saturated and unsaturated soil states. Like most existing models, results from the SCTX test were used to calibrate the model. Since the SCTX test is a drained test, the model capabilities were not investigated under undrained loading conditions. It is worth noting that undrained loading provides a better representation for the coupled hydro-mechanical behavior.

In this paper, recent advancements in both testing and modeling of unsaturated soils are integrated to fully characterize the hydro-mechanical behavior of unsaturated soils under cyclic undrained loading. Two HSTs were developed with different dimensions. Conventional oedometer and direct shear devices for saturated soils were modified and equipped with an HST to measuring suction changes during undrained loadings for unsaturated soils. With the new devices, the testing time reduced from weeks to a few hours. Then, a series of constant water content oedometer and direct shear tests (CWOD and CWDS, respectively) were performed on a compacted silt. Loading–unloading cycles were applied during CWOD testing to investigate both the hydraulic and the mechanical hysteresis behavior. Then, the CWDS results were used to calibrate strength parameters for the model proposed by Riad and Zhang (*74*). Moreover, the K_0 explicit formulation proposed by Zhang et al. (*19*) was utilized to analyze the test results and calibrate stress–strain parameters in the model. The model predictions were then compared with the measured behavior to validate the proposed model.

The paper is organized as follows. First, designs of the new testing equipment are provided and explained in detail. Following this, the testing program is explained in relation to the tested material, testing procedures, and results presentation. Then, a theoretical method is developed to use the results from constant water content tests for constitutive modeling purposes. This is followed by analysis results and discussion. The paper closes with the main conclusions of this work.

New Testing Equipment for Unsaturated Soils

Development of an HST

In this research, an HST was developed according to the principles described by Ridley and Burland (*21*). For oedometer tests, a design similar to that adopted by Li and Zhang (*23*) is utilized here. The HST consists of a pressure transducer, a metal housing, and a high-air-entry (HAE) ceramic disc. The ceramic disc is glued to a stainless steel ring and then glued to the housing. This design, therefore, allows an easy replacement for the ceramic disc when the HST loses its function. The water reservoir has a volume of 0.38 mm^3 located between the HAE ceramic disc and a deformable diaphragm of a pressure transducer. This design, however, was too big for the direct shear cell. Consequently, a miniature HST was developed. The miniature HST comprises (1) a miniature EPB-PW pressure transducer, (2) a 15 Bar HAE disc (6.4 mm in diameter and 1 mm in thickness), and (3) a 0.51 mm^3 water reservoir. Figure 1, *a* and *b*, shows the designs adopted for the large and miniature HSTs, respectively. Figure 1*c* shows a picture of the fabricated HSTs indicating the difference in dimensions. The HSTs were saturated in a closed chamber (Figure 1*d*) by means of applying water pressure cycles of 500 kPa (*21, 23, 75*). It usually takes a week for the first saturation.

After saturation, the HST was calibrated in a positive pressure range. The calibration procedure was done in the closed chamber by applying a very accurate positive pressure to the water in the chamber. Then, the HST readings were compared with the applied pressure, and linear calibration parameters were adopted using the least square method. The calibration parameters can extend to the negative pressure range based on extrapolation (*23, 76*). The calibration accuracy can be considered good when the water pressure drops to −100 kPa immediately after cavitation. The time of suction measurements (i.e., test duration) is influenced by two factors: (a) the time needed for the soil to reach equilibrium and (b) the HST reaction time. For undrained loading, the suction equilibrium time is instantaneous (*77*). Consequently, the suction measurement duration depends solely on the HST reaction time. After calibration, the HST's response time was examined by means of the loading–unloading process, and it was instantaneous, as shown in Figure 1*d*.

Moreover, the maximum attainable suction of the HSTs was determined with a free evaporation test (*22*) and it was was approximately 650 kPa for the large HST and 520 kPa for the miniature HST, as shown in Figure 1*e*. Figure 1*e* indicates a quick drop in pressure to nearly

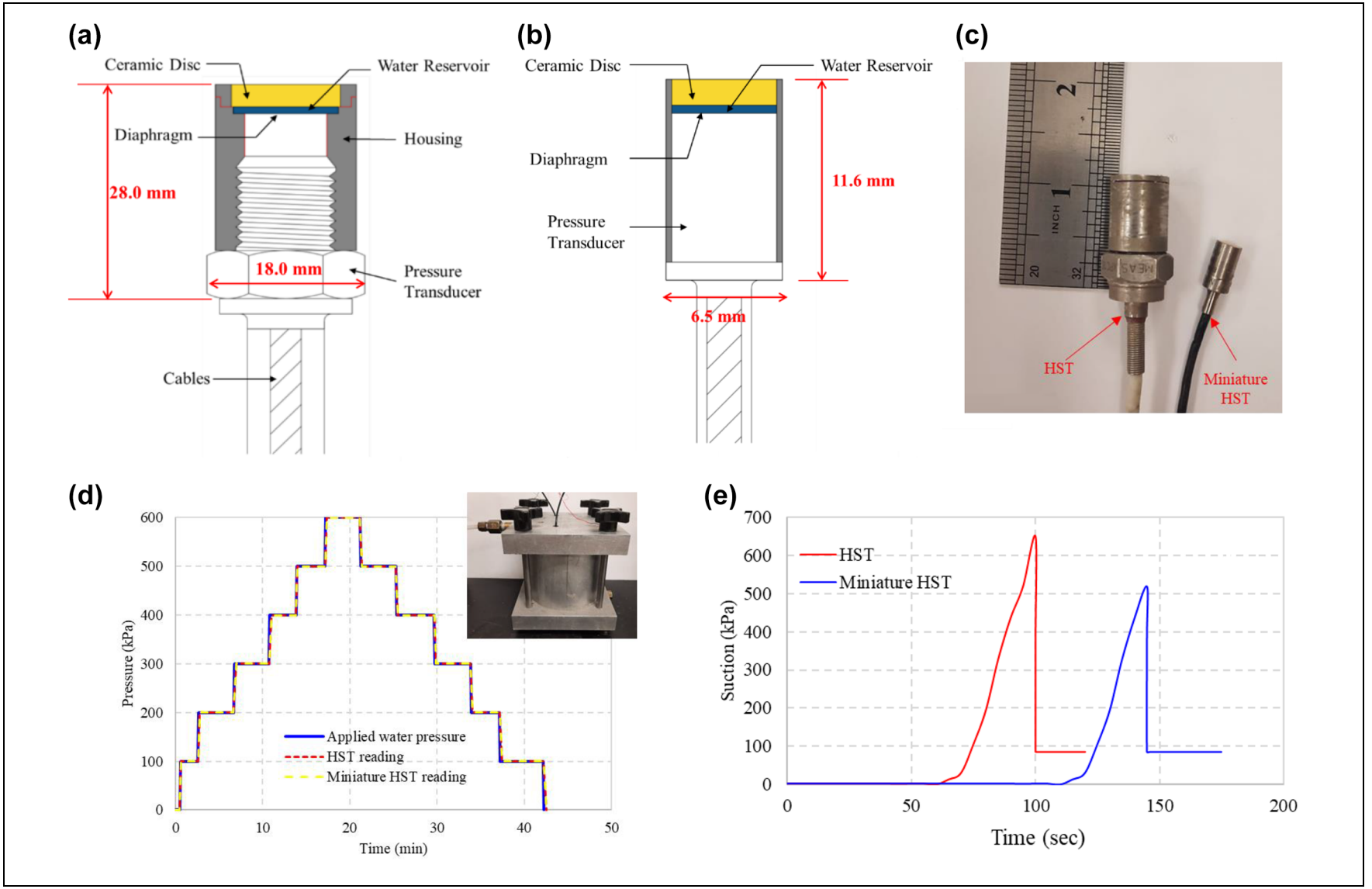

Figure 1. High-suction tensiometer (HST) used in this research: (*a*) HST design, (*b*) miniature HST design, (*c*) HST photographs, (*d*) calibration curve, and (*e*) maximum attainable suction (22).

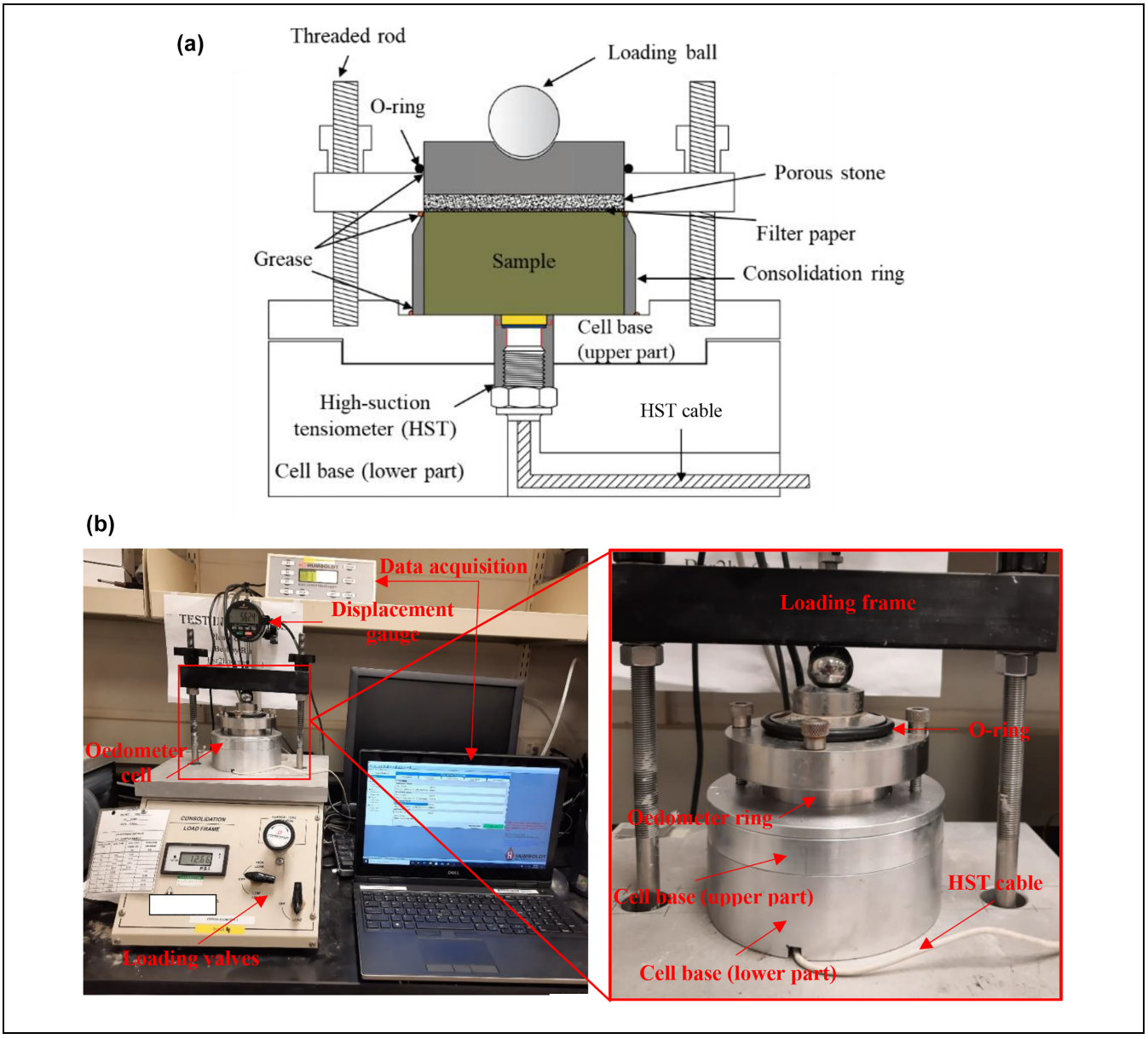

Figure 2. Modified oedometer with high-suction tensiometer (HST): (*a*) schematic plot (after Li et al. [*43*]) and (*b*) pictures of modified oedometer with HST.

−100 kPa, indicating accurate calibration. More details of fabrication, saturation, and calibration of the HST can be found in the work by Li and Zhang (*23*).

Development of New Oedometer Cell

Similar to Zhang et al. (*77*), an HST was mounted at the bottom of a Humboldt oedometer cell. The conventional cell base was replaced with two split parts. The upper part holds the HST cylindrical body. However, the lower part holds the HST cable and hexagonal bolt (Figure 2*a*). This design ensures easy installation and good contact between the HST and soil sample. The rest of the setup was similar to the standard oedometer test for saturated soils. The soil specimen was placed in a standard consolidation ring, as shown in Figure 2*a*. To prevent any evaporation, grease was applied at possible air contact locations, as shown in Figure 2*a*. Similar steps were followed by other researchers (*75, 77*). Figure 2*b* shows a picture of the loading frame with the modified cell.

Development of New Direct Shear Cell

In this step, a conventional direct shear cell was modified for unsaturated soil testing purposes, as shown in Figure 3. The new cell has a modified top-loading cap to

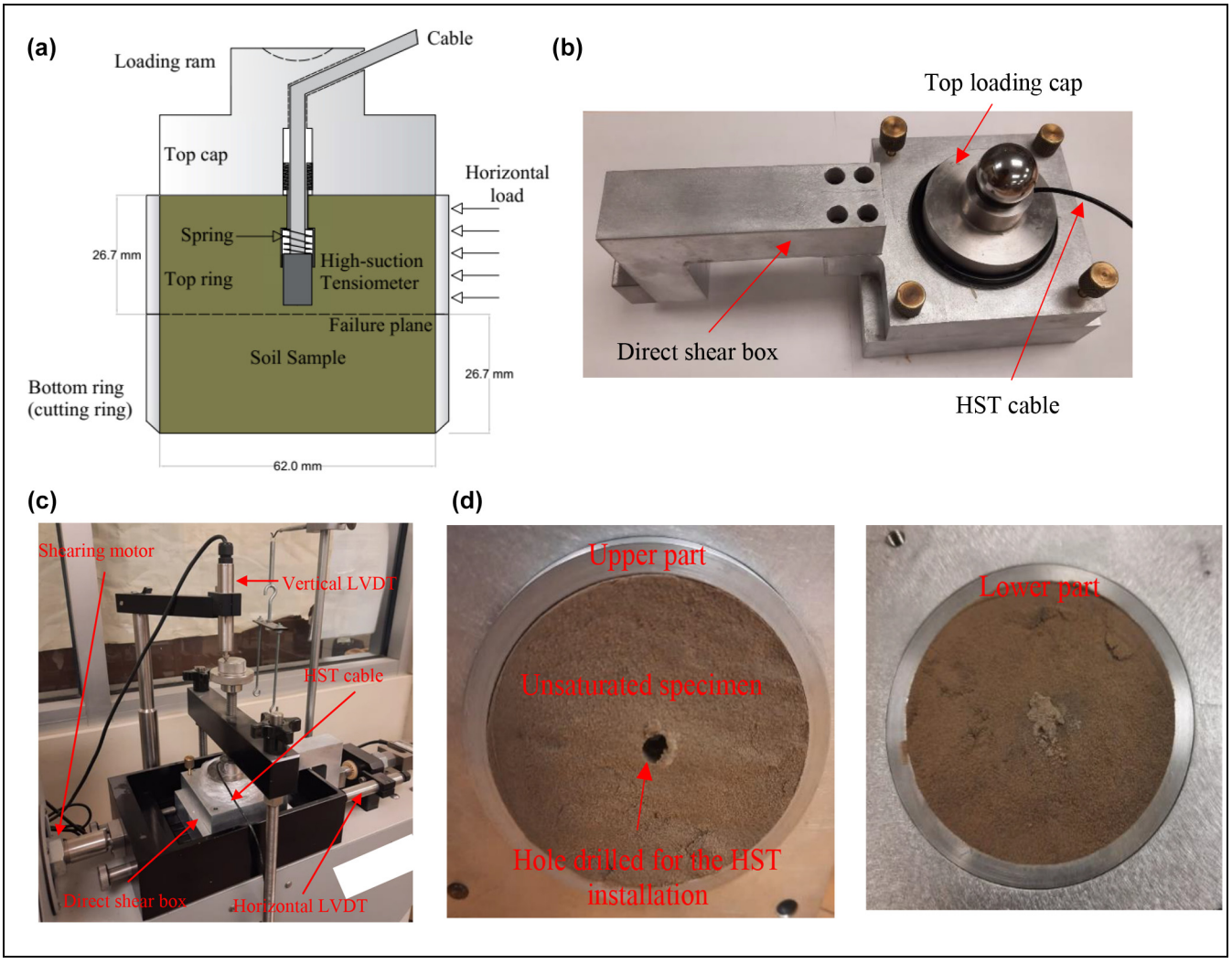

Figure 3. New direct shear test apparatus: (*a*) schematic design, (*b*) photograph of the shear cell, (*c*) direct shear testing system, and (*d*) sheared specimen.
Note: HST = high-suction tensiometer; LVDT = linear variable differential transformer.

host the HST. A metal spring is also used to ensure good contact between the soil and HST during the whole loading process. Figure 3*a* shows a schematic plot of the new cell. For more representative measurement of the soil suction at failure, the miniature HST should be located on the failure plane. However, during real testing, the failure plane is usually rough because of the nonuniformity of the soil specimen. Consequently, the HST tip was set to be approximately 1 mm above the failure plane, as shown in Figure 3*a*. This design ensures representative suction measurements without affecting the soil shear behavior. This new cell was designed to accommodate the conventional direct shear box. Therefore, this new cell can be placed in the conventional direct shear box, as shown in Figure 3*b*. With this new cell, the test can be performed in any conventional direct shear apparatus, as shown in Figure 3*c*. Figure 3*d* shows a soil specimen after shearing in which the HST was nearly at the failure plane.

Testing Program

Materials, Specimen Preparations, and Testing Procedures

The unsaturated soil specimens were fabricated using silt soil collected from the Missouri riverbed. The soil was sieved and classified as silty sand (SM) as per the Unified Soil Classification System (USCS). The collected soils were oven-dried and pulverized, and only those passing sieve No. 200 (i.e., silty soil) were used in this study. The collected fines (silt) had the following properties: optimum moisture content (w_{opt}) of 12%, maximum dry density of 17.0 kN/m^3, a specific gravity of 2.7, and it was

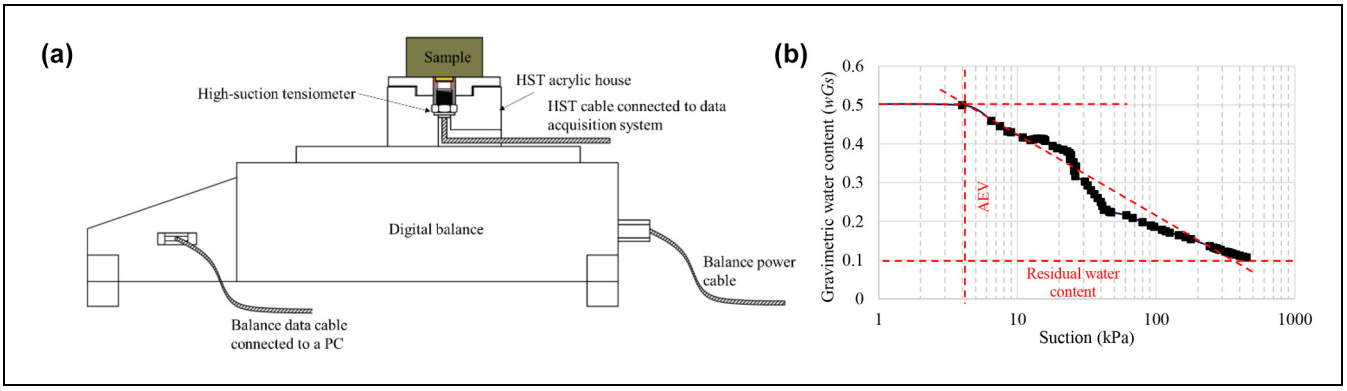

Figure 4. Soil–water characteristic curve (SWCC): (*a*) schematic plot for the used system and (*b*) measured SWCC.
Note: HST = high-suction tensiometer; PC = personal computer; AEV = Air Entry Value.

non-plastic. The soil was then mixed with distilled water at the optimum moisture content. To ensure moisture equilibrium, the mixed soil was stored in well-sealed plastic bags for at least 2 days.

For the soil–water characteristic curve (SWCC), the soil was compacted at the optimum moisture content in a consolidation ring. The soil was then saturated with distilled water for 1 week; then, a calibrated HST was used to ensure saturation (i.e., zero suction) at different locations of the soil sample. The SWCC was determined using an HST and balance following the procedure described by Toll et al. (*36*). This procedure was also adopted by Li et al. (*40*) to measure the water retention and shrinkage curves simultaneously. They measured the soil suction, water content, and volume changes during testing to construct both curves. Figure 4*a* shows a schematic plot for the system used to detect the SWCC. The sample was continuously exposed to air, and the HST and balance allowed for continuous measurement of suction and soil weight. At the end of the test, the sample dry mass was detected by oven drying. The dry mass allowed for calculating the moisture content corresponding to every soil weight. Figure 4*b* shows the SWCC measured for this soil. It is worth noting that the testing time was reduced to 24 h instead of 15 days for typical soils using the pressure plate method. The air-entry suction value and residual water content for this soil were determined to be approximately 3.2 kPa and 0.1, respectively.

The soil was then dynamically compacted as per ASTM D1557 (*78*). For the constant water content oedometer (CWOD), the consolidation rings were then used to cut the soil to minimize disturbance. After cutting, the soil specimens were exposed to air for different periods to reach different moisture (suction) levels. Then, soil specimens were stored in a sealed container for 1 week to reach moisture equilibrium. After that, the saturated HST was installed into the oedometer base, as shown in Figure 2*a*. To avoid cavitation during preparation, the HAE disc of the HST was covered with a thin layer of kaolin paste. Then, the unsaturated soil specimen was placed on top of the HST, as shown in Figure 2*a*. The self-weight of the soil specimen and ring allowed good contact between the HST and the bottom of the specimen. The oedometer cell was then placed under the loading frame, as shown in Figure 2*b*. The vertical displacement was measured by a digital indicator with an accuracy of 0.000254 cm and a range of 2.54 cm. The indicator and the HST were connected to an automated data logger for continuous measurement of vertical displacement and suction, at 2 s intervals, throughout the CWOD test.

During the CWOD test, the loads were applied in steps of 12.5, 25, 50, 100, 200, 400, 800, 1600, and 3000 kPa of vertical stress. Then, cycles of loading and unloading were applied between 800 and 12.5 kPa. The specimens were unloaded to 12.5 kPa before the test was terminated. The sample was allowed to reach both suction and vertical displacement equilibrium for every loading or unloading level. The equilibrium usually takes 15 to 30 min. The stabilized suctions and vertical displacements were used as final values for each load level. Depending on the initial soil suction and the number of loading–unloading cycles, it normally took 7 to 13 h to complete a test. To ensure constant water content, the weight of the soil specimen was measured before and after testing.

For the CWDS test, split rings (53.4 mm in height and 62.0 mm in diameter) were used to cut the soil specimens. The specimens were prepared in the same way as those for the CWOD tests. After conditioning, the specimens were placed in the direct shear box, as shown in Figure 3*b*. Also, the saturated miniature HST was assembled with the top cap, as shown in Figure 3*a*. Before HST installation, a hole of 6.5 mm in diameter and 25.7 mm in depth was drilled at the specimen center. A thin layer of saturated kaolin was also used to smear the ceramic disc

to prevent cavitation. After installation, the shear box was then placed in the shearing machine, as shown in Figure 3*c*. A linear variable differential transformer (LVDT) was mounted at the top of the soil to monitor the soil volume. Then various normal loads were applied. Normal loading also changes the soil suction; then, the sample was allowed to reach equilibrium. When the tensiometer reading stabilized, the direct shear load was applied at a constant loading rate of 0.05 mm/min until failure. The soil specimen after the direct shear test was then used for moisture content measurement.

Presentation of Test Results

CWOD. Figure 5 shows the typical response of a soil specimen ($w = 10.92\%$) during a CWOD test. The initial suction value was 24.60 kPa as shown on Figure 5 and the corresponding σ_v was 12.5 kPa. For each applied load as shown in Figure 5*a*, there were corresponding instantaneous changes in settlement, degree of saturation, and suction, followed by an equilibrium stage as shown in Figure 5, *b*–*d*, respectively. An enlarged plot for the suction changes with time is provided in Figure 5*d*. This plot clearly shows the gradual decrease or increase in suction with increments or decrements of loading, respectively. The degree of saturation was back-calculated using the intrinsic relationship ($S_r = wG_s/e$) with known void ratio and water content. Figure 5*d* shows that when the specimen is first loaded or unloaded, suction jumps to high or low values before reaching equilibrium. Since water and soil solids are not compressible, the equilibrium time was most likely related to either internal redistribution of the water, or drainage of the pore air, or both. The sample then takes a few minutes to reach internal stability in respect of suction, which was captured by the HST. Sometimes suction jumps to a negative value (positive water pressure), but it stabilizes to positive values at the end. The soil suction after stabilization differs from the previous value before loading or unloading. It can be seen in Figure 5 that there were irrecoverable volume changes during unloading. The vertical displacements did not recover to their initial values, and the stabilized suction was lower than that in the loading process at the same σ_v level.

The stabilized measurements were then reported as the final values at the corresponding stress level. Figure 6, *a*–*c*, shows the specific volume ($v = 1 + e$, where e is void ratio), degree of saturation (S_r), and suction (s) versus the vertical stress curves for six CWOD tests. Because of the wide suction range, suction versus vertical stress curves are presented in two separate $s - \sigma_v$ plots for better visualization. The test at $w = 8.0\%$ was terminated after one loading–unloading cycle because of HST loss of function. As shown in Figure 6*a*, specific volume slowly

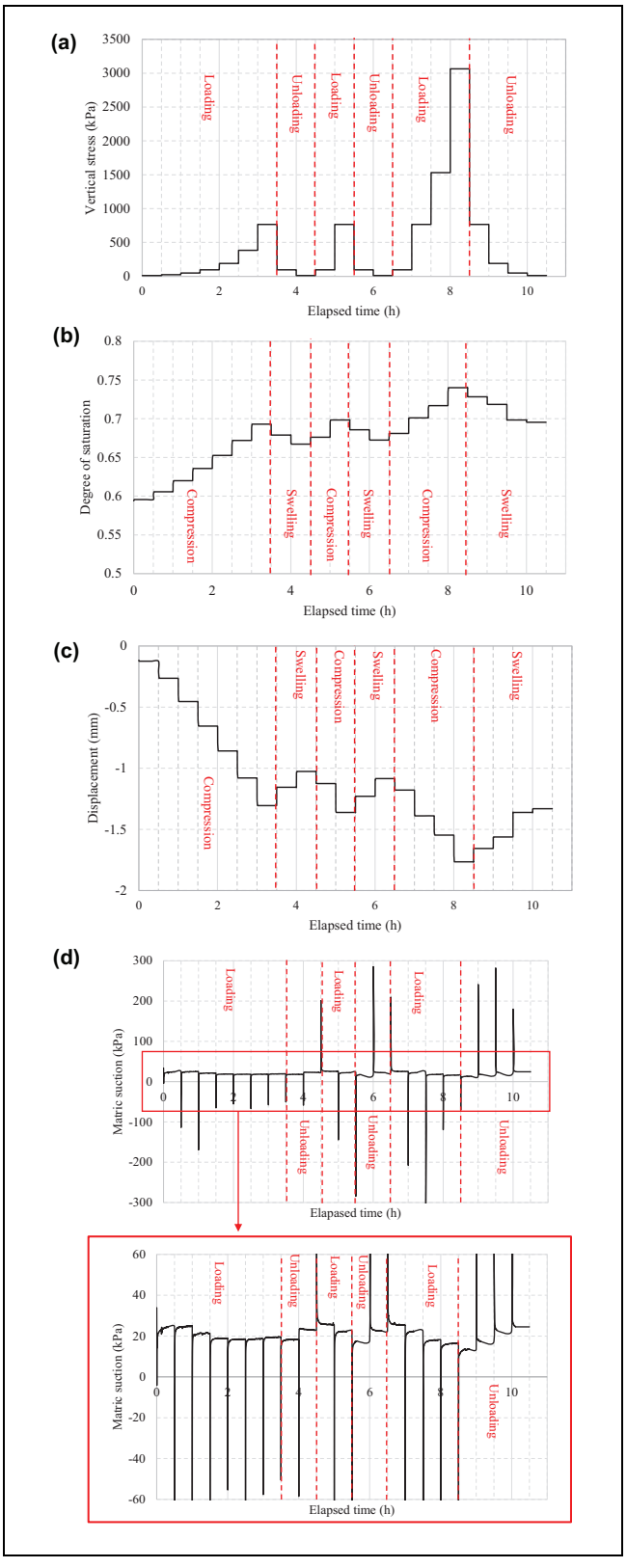

Figure 5. Typical responses of a soil specimen during the constant water content oedometer test ($w = 10.92\%$): (*a*) applied loads, (*b*) measured vertical displacement, (*c*) degree of saturation, and (*d*) measured matric suction.

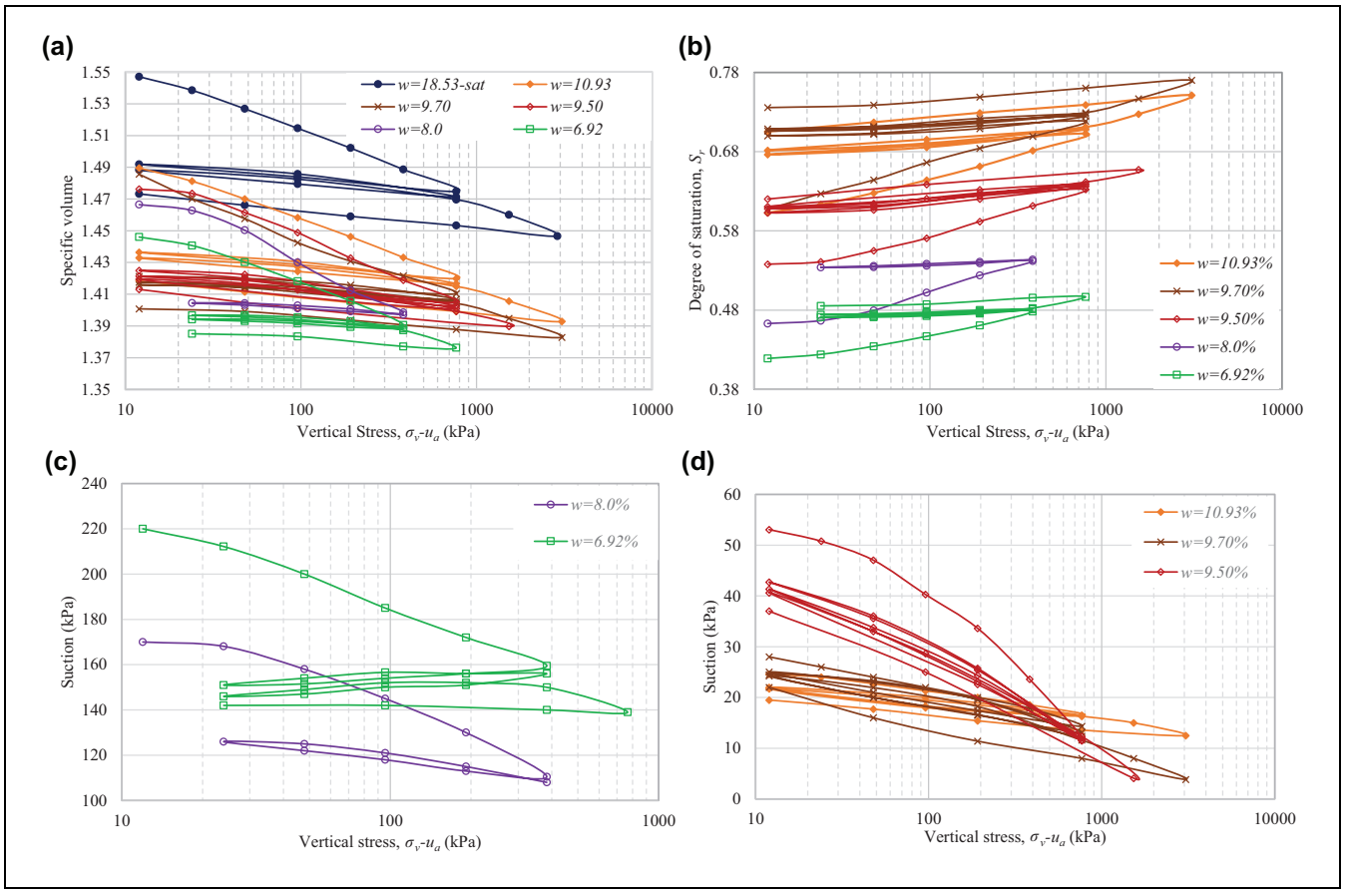

Figure 6. Soil responses during constant water content oedometer tests: (*a*) void ratio versus applied vertical stress, (*b*) degree of saturation versus applied vertical stress, (*c*) soil suction versus applied vertical stress (w = 8% and 6.92%), and (*d*) soil suction versus applied vertical stress (w = 10.93%, 9.7%, and 9.5%).

decreased with σ_v at less than 30 kPa. A limited transition zone was noticed at σ_v between 30 and 60 kPa, while the decrease then became steeper when σ_v was greater than 60 kPa. During unloading, all specimens unloaded along less steep and almost parallel lines, indicating irrecoverable volume changes. A hysteresis behavior was also noticed during the loading–unloading cycles. The CWOD is, in fact, an undrained compression test. As shown in Figure 6*c*, every test started from the equalization suction corresponding to the specimen's moisture content. During loading, suction decreased, and the degree of saturation increased. Such behavior better represents the hydro-mechanical coupling of the soil than the suction-controlled test. Then, as the soil was subjected to an unloading process, suction increased. If the soil was reloaded, both the void ratio and suction decreased by following new curves, indicating that there were hystereses in both mechanical and hydraulic behavior of the unsaturated soil.

The degree of saturation had opposite behavior to that of the specific volume as shown in Figure 6*c*. It increased with loading and decreased with unloading. Figure 6 indicates that the higher the initial moisture content, the higher the initial void ratio, the higher the degree of saturation, and the lower is the initial suction. Soils with higher initial moisture content were more compressible than those that were drier, which is reasonable because suction is known to have stiffening effects on unsaturated soils. For the saturated oedometer test (w = 18.5%), degree of saturation (S_r = 1) and suction (s = 0) are plotted in Figure 6*b* for better visualization.

CWDS. CWDS tests were conducted at nine constant water content levels with different normal stress levels. Figure 7 shows the shear stress and volumetric strain changes during shearing. The soil information before testing and at failure is summarized in Table 1. It was noticed that, roughly, when normal stress was less than 100 kPa, suction increased during shearing. This can be attributed to dilative shear behavior, as shown in Figure 7*b*. However, contractive behavior was noticed at normal stresses higher than 100 kPa, and, consequently, suction decreased during shearing. It is worth noting that,

Table 1. Summary of Specimens' Initial and Final Conditions for Direct Shear Tests

	Initial condition			At failure condition		
Test no.	*w* (%)	*v*	*s* (kPa)	*s* (kPa)	Shear strength (kPa)	Normal stress (kPa)
1	11.08	1.52	45.5	50.0	109.8	95.8
2	10.95	1.49	32.0	48.6	85.4	95.8
3	10.59	1.47	20.4	29.1	22.2	23.9
4	10.50	1.46	6.4	12.9	35.4	47.9
5	9.63	1.45	50.0	25.0	138.3	191.5
6	9.54	1.45	57.0	50.8	16.3	47.9
7	9.45	1.44	64.4	15.0	134.8	191.5
8	9.07	1.43	40.4	–62.9	291.7	383.0
9	8.42	1.42	115.0	29.5	197.5	287.3

Note: no. = number.

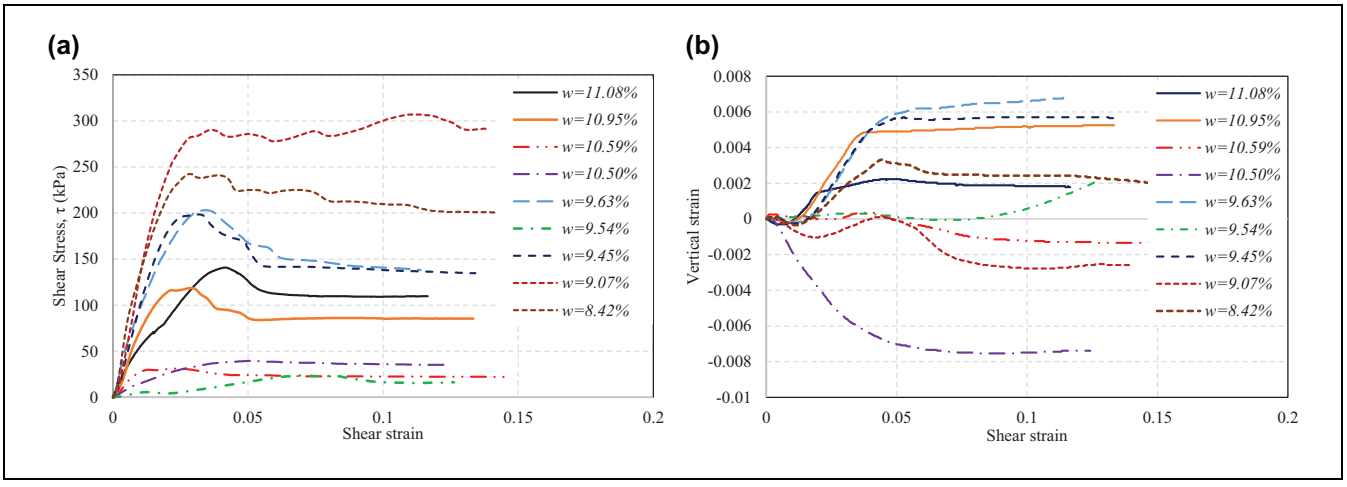

Figure 7. Constant water content direct shear test results: (*a*) shear stress versus shear strain and (*b*) vertical strain versus shear strain.

for test# 8 (w = 9.07%), a negative suction value (positive pore water pressure) was noticed as a result of the high normal stress applied (383.1 kPa). As the horizontal displacement increased, the shear stress increased until a peak was reached and then stabilized or decreased. Generally, the ultimate shear stresses increased with increasing normal stress, which is typical for most soils.

Theoretical Analysis of Test Results

Overview of the MSSA

Based on a detailed qualitative study of soil behavior in the *v-p-q-s* space, Zhang and Lytton (*69*) divided the soil volumetric behavior into elastic and plastic surfaces based on the following criteria:

1) The shape and position of the plastic hypersurface are always fixed in the *v-p-q-s* space for a given soil.
2) The shape and position of the elastic surface remain fixed during elastic loading and unloading.
3) During plastic loading, the position of the elastic surface changes (i.e., moves downward). However, its shape remains the same.
4) The yield curves are the intercepts of the elastic and plastic surfaces.

Later, Zhang and Lytton (*71*) extended the MSSA to study the hydro-mechanical behavior of unsaturated soils. Considerable attention was paid to the consistency between different soil phases (i.e., soil solid, water, and air). They came up with the following consistency requirement/principles for any coupled model: (a) the degree of saturation, S_r, and water content, wG_s, are closely related to the void ratio, e, and should be coupled; (b) elastoplasticity is a material behavior while S_r, wG_s, and e are representatives of such behavior and, consequently, should be simultaneously elastic or elastoplastic and share the same yield surface; (c) the plastic

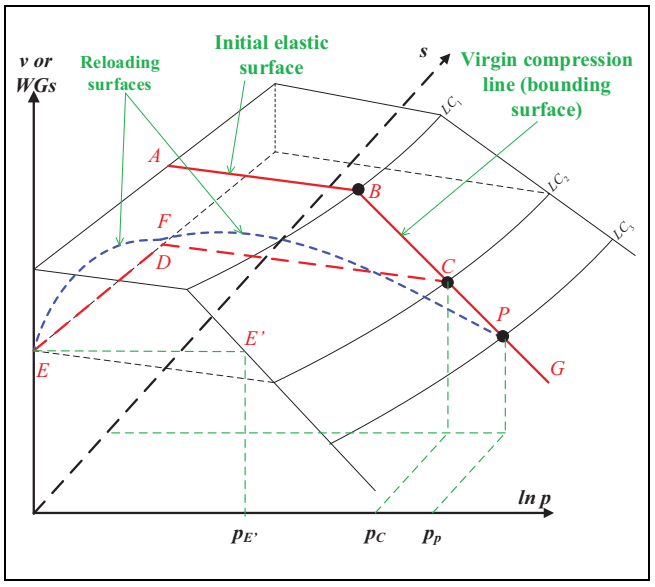

Figure 8. 3D representation for soil hysteresis behavior (modified state surface approach).

volumetric strains are exactly equal to the plastic water content changes; and (d) the air phase behavior is always elastic.

Recently, Riad and Zhang (*73*) further extended the MSSA to study the hydro-mechanical behavior of unsaturated soils considering both hydraulic and mechanical hysteresis. The MSSA was extended based on three main principles (refer to Figure 8): (a) the reloading surface starts at the elastic unloading surface (point E) and ends at the plastic surface (point P); (b) the intersection between reloading and plastic surfaces is a new yield curve (point P on LC_3 yield curve); and (c) the intersection yield curve location depends on how much further the sample was unloaded in relation to mean net stress or suction.

3D Elastoplastic Hydro-Mechanical Model: Overview

Based on the coupled MSSA (after extension in Riad and Zhang [*73*]), Riad and Zhang (*74*) developed a new elastoplastic model that can predict the coupled hydro-mechanical hysteresis behavior for unsaturated soils in a consistent manner (referred to as the C3DHM model hereafter). The mechanical part of the model is the same as the BBM (*46*), while new equations were proposed for the hydraulic behavior, as shown later. The model has one major superiority over other models, that is, it uses one yield surface only to simulate mechanical and hydraulic behavior simultaneously, which ensures consistent predictions for the mechanical and hydraulic behaviors.

The C3DHM was formulated in relation to surfaces using the MSSA as follows. Equations 1 and 2 show the elastic and plastic surfaces for the specific volume, and Equations 3 and 4 show the specific water volume, $v_w = 1 + e_w = 1 + wG_s$ elastic and plastic surfaces, under triaxial loading conditions (for equation notation, please see the notation list in Table 3).

$$v^e = C_1 - \kappa \ln p - \kappa_s \ln(s + p_{at}) \tag{1}$$

$$v = C_2 - \kappa_s \ln\left(\frac{s + p_{at}}{p_{at}}\right) - \kappa \ln\left(\frac{p}{p^c}\right) - (\lambda(s) - \kappa) \left[\ln\left(p + \frac{q^2}{M^2(p + ks)}\right) - \ln(p^c)\right] \tag{2}$$

$$v_w^e = C_2 - \kappa_w(s) \ln\left(\frac{s + p_{at}}{p_{at}}\right) - \lambda_{w1}(s) \ln\left(\frac{p}{p^c}\right) + [\lambda_{w2}(s) - \kappa] \ln\left(\frac{p}{p_0}\right) \tag{3}$$

$$v_w = C_2 - \kappa_w(s) \ln\left(\frac{s + p_{at}}{p_{at}}\right) - \lambda_{w1}(s) \ln\left(\frac{p}{p^c}\right) + (\lambda_{w2}(s) - \kappa)\left[\ln(p) - \ln\left(p + \frac{q^2}{M^2(p + ks)}\right)\right] \tag{4}$$

where $\lambda(s) = \lambda(0)[(1 - r)\exp(-\beta s) + r]$, $\kappa_w(s) = \kappa_w(0)[(1 - a)\exp(-bs) + a]$, $\lambda_{w1}(s) = \lambda(0)[(1 - c)\exp(-ds) + c]$, and $\lambda_{w2}(s) = \lambda(0)[(1 - g)\exp(-fs) + g]$.

At zero suction, Equations 3 and 4 became the same as Equations 1 and 2, respectively. This feature ensures a smooth transition between saturated and unsaturated states. Including the deviatoric stress, q, in Equations 4 and 2 allowed for simulating the hydro-mechanical coupling during shearing. This feature is rarely constituted in most existing models for unsaturated soils. During unloading, for simplicity, the C3DHM model is fully compatible with the BBM (represented by Equations 1 and 3). However, during reloading, the bounding surface concepts (*79, 80*) were applied to capture the hysteretic behavior. Equation 5 was then proposed for the specific volume reloading surface.

$$v^r = C_3 - \kappa_s \ln\left(\frac{s + p_{at}}{p_{at}}\right) - \kappa \ln\left(\frac{p}{p^c}\right) - f(\delta, p)(\lambda(s) - \kappa) \ln\left(\ln\left(p + \frac{q^2}{M^2(p + ks)}\right) - \ln(p)\right) \tag{5}$$

where $f(\delta, p) = p\delta/\left(p\delta + A(1 - \delta)^B\right)$ is a function representing the distance between the current yield surface and the bounding surface, and $\delta = p^*{}_0/(p^*{}_0)_B$ is the ratio between current preconsolidation pressure, $p^*{}_0$, and preconsolidation pressure on the bounding surface, $(p^*{}_0)_B$. It is worth noting that the value of δ is increasing from the current value to 1 during reloading (or drying).

Constant C_3 in Equation 5 can be calculated from the initial reloading conditions (point E in Figure 8), as $C_3 = C_1 + \kappa_s \ln(p_{at}) + \kappa \ln(p^c)$. It is worth noting that p_0 can be usually calculated from Equation 5 and plugged into Equation 3 to reproduce the hydraulic hysteresis. Consequently, no additional equations (i.e., model parameters) are required to represent the hydraulic hysteresis. The model was successfully used to simulate the hysteresis behavior of unsaturated soils under drained loading (i.e., from the SCTX test).

The incremental forms were then derived from the surfaces' equations. The elastic volumetric ($d\varepsilon_v^e$) and hydraulic ($d\varepsilon_w^e$) strains (i.e., elastic water content changes) resulting from s and p changes can be derived as follows:

$$d\varepsilon_v^e = \frac{\kappa}{v_0}\frac{dp}{p} + \frac{\kappa_s}{v_0}\frac{ds}{s + p_{at}} \tag{6}$$

$$\begin{aligned} d\varepsilon_w^e = {} & \frac{(\lambda_{w1}(s) + \lambda_{w2}(s) - \kappa)}{v_0}\frac{dp}{p} \\ & + \left[\frac{\kappa_w(s)}{s + p_{at}} + \frac{\partial \kappa_w(s)}{\partial s}\ln\left(\frac{s + p_{at}}{p_{at}}\right)\right. \\ & \left. + \frac{\partial \lambda_{w1}(s)}{\partial s}\ln\left(\frac{p}{p^c}\right) - \frac{\partial \lambda_{w2}(s)}{\partial s}\ln\left(\frac{p}{p_0}\right)\right]\frac{ds}{v_0} \end{aligned} \tag{7}$$

The elastic shear strain was not included in the surface equations, but the conventional Equation 8 was used.

$$d\varepsilon_s^e = \frac{dq}{3G} \tag{8}$$

The complexity in Equation 7 was attributed to the model's ability to capture the non-linear hydraulic behavior. Another reason is the simple equations that are used to predict the plastic hydraulic strains (i.e., plastic water content changes), as shown in the rest of this section. The plastic volumetric ($d\varepsilon_v^p$) and hydraulic ($d\varepsilon_w^p$) strains can be calculated as follows:

$$d\varepsilon_v^p = \frac{\lambda(s) - \kappa}{v_0}\frac{dp^*{}_0}{p^*{}_0} \tag{9}$$

$$d\varepsilon_w^p = \frac{\lambda_{w2}(s) - \kappa}{v_0}\frac{dp^*{}_0}{p^*{}_0} \tag{10}$$

Equations 9 and 10 can be used to derive the hydro-mechanical coupling equations as follows:

$$\frac{dp_0}{p_0} = \frac{v_0}{\lambda_{w2}(s) - \kappa}d\varepsilon_w^p = \frac{v_0}{\lambda(s) - \kappa}d\varepsilon_v^p \tag{11}$$

In this model, the shape of the yield surface is assumed to be the same for both hydraulic and mechanical behaviors. Thus, the model adopts the yield hypersurface proposed in the BBM, Equation 12. Accordingly, the flow rule can be formulated as shown in Equation 13.

$$q^2 - M^2(p + ks)(p_0 - p) = 0 \tag{12}$$

$$\begin{aligned} d\varepsilon_s^p &= \frac{2q\alpha}{M^2(2p + ks - p_0)}d\varepsilon_v^p \\ &= \frac{2q\alpha}{M^2(2p + ks - p_0)}\frac{\lambda(s) - \kappa}{\lambda_{w2}(s) - \kappa}d\varepsilon_w^p \end{aligned} \tag{13}$$

Up to Equation 13, the model covered all the hydro-mechanical features and coupling under monotoning loading conditions. However, during reloading (or drying), the soil behavior (mechanical and hydraulic) is not purely elastic and contains a plastic item. The plastic strains during reloading (or drying) can be calculated using Equation 14. It is worth noting that Equation 14 converges to Equation 9 when the soil reaches the boundary surface ($\delta = 1$).

$$d\varepsilon_v^p = d\varepsilon_w^p = f(\delta, p)\frac{\lambda(s) - \kappa}{v_0}\frac{dp^*{}_0}{p^*{}_0} \tag{14}$$

The C3DHM model requires 19 model parameters to fully simulate the elastoplastic hydro-mechanical behavior with consideration of both mechanical and hydraulic hysteresis—which is eight parameters more than the original BBM. Two of them are related to the shear strength behavior of the soil and the rest are for the coupled hydro-mechanical hysteresis behavior. Thus, the shear strength parameters are calibrated first, using results from CWDS tests.

Parameter Calibration Procedure

Shear Strength Parameters. For saturated soils, the Mohr–Coulomb failure criterion leads to a linear relationship between the shear strength and normal effective stress. However, for unsaturated soils, besides the net normal stress, suction also affects the soil strength (*4, 81–83*). Assuming shear strength is a linear function of net normal stress and suction, Fredlund et al. (*83*) proposed Equation 15.

$$\tau_f = c' + \left(\sigma_f - u_a\right)_f \tan\phi' + \left(u_a - u_w\right)_f \tan\phi^b \tag{15}$$

By knowing the soil stress state at failure (i.e., $(\sigma_n - u_a)_f$, $s_f = (u_a - u_w)_f$, and τ_f) for every test, shown in Table 1, linear regression was performed to calibrate the shear strength parameters for Fredlund et al.'s (*83*) failure envelope, Equation 15. The least-squares method can be applied to estimate a suitable combination of parameters, as follows: $c' = 0kPa$, $\phi' = 36.16^0$, and $\phi^b = 8.10^0$. To increase the coefficient of determination ($R^2 = 98.2\%$), it is worth noting that a suction value of zero is considered for test# 8 ($w = 9.07\%$) instead of the negative value. For elastoplastic modeling, Riad and

Table 2. Calibrated Model Parameters

Parameter	Unit	Best fit value	Parameter	Unit	Best fit value
C_2	na	0.466	$\kappa_w(0)$	na	0.001
κ_s	na	0.005	a	na	0.072
κ	na	0.003	b	MPa^{-1}	41.76
$\lambda(0)$	na	0.18	c	na	0.013
r	na	0.002	d	MPa^{-1}	119.63
β	MPa^{-1}	1.503	e	na	0.102
p^c	MPa	3.17E−5	f	MPa^{-1}	99.64
M	na	1.47	A	na	1.266
k	na	0.19	B	na	0.009
α	na	0.794	μ	na	0.35

Note: na = not applicable.

Zhang (*74*) adopted the shear strength equation proposed in the BBM, as follows:

$$q = M(p + ks) \tag{16}$$

In Equation 16, the effective cohesion (c') of the soil, is commonly assumed to be zero. Mathematically, the BBM shear strength parameters can be derived from Fredlund et al.'s (*83*) Equation 15 as follows:

$$M = \frac{3(K_p - 1)}{2 + K_p} \tag{17}$$

$$k = \frac{2\tan\phi^b\sqrt{K_p}}{K_p - 1} \tag{18}$$

$K_p = \tan^2\left[\frac{\pi}{4} + \frac{\phi'}{2}\right]$.

Then, the BBM shear strength parameters can be calculated from ϕ' and ϕ^b to be $M = 1.47$ and $k = 0.19$.

Stiffness Parameters. As mentioned earlier, recently, Zhang et al. (*19*) derived an explicit formulation of the at-rest coefficient of unsaturated soils. Accordingly, methods were also developed to use the SCOD (*19*) and CWOD tests (*77*) for constitutive modeling purposes. It is worth noting that, in both cases, the shear strength parameters were calibrated from oedometer tests results, which does not mobilize the soil strength. Consequently, these parameters are extrapolations of the test results to failure conditions and may be subject to significant error. Moreover, the proposed procedures can be utilized to calibrate parameters related to mechanical behavior only. Since the mechanical behavior in the C3DHM model is exactly similar to the BBM, the equations derived by Zhang et al. (*19*) for calibrating the mechanical parameters in the BBM can be used here. However, the calibration procedure needs to be extended to calibrate the hydraulic and hysteresis parameters.

In the oedometer test, the condition of zero lateral strain leads to the ratio between total volumetric, ε_v, and shear strain, ε_s, increments being, as in Wood (*84*):

$$\left(\frac{\delta\varepsilon_v}{\delta\varepsilon_s}\right)_{k_0} = \left(\frac{\delta\varepsilon_v^e + \delta\varepsilon_v^p}{\delta\varepsilon_s^e + \delta\varepsilon_s^p}\right)_{k_0} = \frac{3}{2} \tag{19}$$

where superscripts "e" and "p" refer to the elastic and plastic strains, respectively. Equation 19 can be used to derive a solution for K_0 corresponding to any critical state soil model (*85, 86*). Using the volumetric and shear strain equations in the BBM (similar to Equations 6, 8, 9, and 13 in this paper), Zhang et al. (*19*) derived Equations 20 and 21 for K_0 in the elastic and plastic zones, respectively.

$$d(\sigma_3 - u_a) = \frac{\mu}{1-\mu}d(\sigma_1 - u_a) - \frac{\kappa_s}{\kappa}\frac{1-2\mu}{1-\mu}\frac{p}{1+p_{at}}ds \tag{20}$$

$$d(\sigma_3 - u_a) = \frac{\left\{\left[(D - EB) - \left(\frac{2\kappa}{3p} + \frac{EA}{3}\right)\right]d(\sigma_1 - u_a) - \left[\frac{2\kappa_s}{s + p_{at}} - EC\right]ds\right\}}{2\left[\frac{2\kappa}{3p} + \frac{EA}{3}\right] + (D - EB)} \tag{21}$$

where

$A = \frac{\lambda(s)-\kappa}{q^2 + M^2(p+ks)p}$

$B = \frac{M^2(p+ks)^2 - q^2}{p + ks}$

$C = \frac{Aq^2k}{q+ks} + \lambda(0)(1-r)\beta\exp(-\beta s)\left[\ln\left(\frac{\lambda(s)-\kappa}{AM^2(p+ks)}\right) - \ln p^c\right]$

$D = \frac{2(1+\mu)}{3(1-2\mu)}\frac{\kappa}{p}$

$E = \left(2 - \frac{6q(p+ks)\alpha}{M^2(p+ks)^2 - q^2}\right)$

Equations 20 and 21 define the K_0 stress path for the C3DHM model in the elastic and plastic zones, respectively. In Equations 20 and 21, the lateral stresses are expressed as increments of vertical stress and suction,

Table 3. List of Notations

Notation	Definition
C_1, C_2, C_3, C_4, and C_5	Constant
$N(s)$	Specific volume at $p = p^c$
q	Deviatoric stress
p	Mean net stress
u_w	Pore water pressure
S_r	Degree of saturation
u_a	Pore air pressure
s	Suction
n	Porosity
e	Void ratio
e_0	Initial void ratio
v^e	Elastic specific volume
v	Total specific volume
e_w	Water ratio = wG_s
v_w^e	Elastic specific water volume = $1 + e_w^e$
v_w	Specific water volume = $1 + e_w$
μ	Poisson's ratio
e	Void ratio
σ_m	Total mean stress
κ	Slope of the unloading–reloading line associated with the mean net stress
κ_s	Slope of the unloading–reloading line associated with soil suction
p_{at}	Atmospheric pressure
$\lambda(s)$	Slope of the virgin expansion line associated with the mean net stress
p^c	Reference stress
λ_s	Slope of the virgin compression line associated with soil suction
$\lambda(0)$	Slope of the virgin compression line associated with the mean net stress for $s = 0$
r	Parameter controlling the slope of the virgin compression line
β	Parameter that controls the slope of the virgin compression line for $s \neq 0$
w	Gravimetric water content
G_s	Soil specific gravity
λ_w	Slope of the normal consolidation for the water phase under a constant matric suction
λ_{ws}	Slope of the segment beyond the yield suction on the soil–water characteristic curve under a constant net normal stress
κ_w	Slope of the unloading–reloading segment in the wG_s versus lnp curve for isotropic compression test at constant suction
H	Soil hardening parameter
A	Model parameter
B	Model parameter
e^r	Void ratio during reloading
p_i	Initial mean net stress
s_i	Initial matric suction
p_0^*	Preconsolidation stress for saturated conditions
p_0	Preconsolidation stress
s_0	Hardening parameter of the suction increase yield curve
p_s	Soil cohesion
M	Slope of the critical state line
k	Parameter describing the increase in cohesion with suction
G	Shear modulus
α	Non-associativity parameter
$\kappa_w(s)$	Slope of specific water volume unloading–reloading line associated with the mean net stress
$\lambda_{w1}(s)$	Slope of the specific water content plastic line associated with the mean net stress
$\lambda_{w2}(s)$	Parameter representing the effect of the yield curve evolution on the specific water volume
$\kappa_w(0)$	Slope of specific water volume unloading–reloading line associated with the mean net stress at saturated conditions
a, b, c, d, f, and g	Soil parameters controlling the hydraulic behavior caused by mean net stress and suction changes
ε_v^e, ε_v^p,and ε_v	Elastic, plastic, and total volumetric strains
ε_s^e, ε_s^p,and ε_s	Elastic, plastic, and total shear strains
ε_w	Hydraulic strains = $dv_w/(1 + e_0)$
ε_w^e and ε_w^p	Elastic and plastic hydraulic strains

(continued)

Table 3. (continued)

Notation	Definition
ε_{vs}^{e} and ε_{ws}^{e}	Elastic volumetric and hydraulic strains caused by suction changes
ε_{vp}^{e} and ε_{wp}^{e}	Elastic volumetric and hydraulic strains caused by mean net stress changes
ε_{v}^{p} and ε_{w}^{p}	Plastic volumetric and hydraulic strains
c'	Effective cohesion
ϕ'	Angle indicating the increase in shear strength with suction
ϕ^{b}	Angle of internal friction associated with net normal stress
$(\sigma_f - u_a)_f$	Net normal stress at failure
$(u_a - u_w)_f$	Suction at failure

which can be measured using the modified CWOD device used in this paper, as shown in Figure 6*c*. Therefore, results from the CWOD test combined with Equations 20 and 21 can be used to calculate the lateral stress. Once the lateral stress is known, the oedometer test becomes a triaxial test with a known stress path. Consequently, a K_0 test (CWOD test) can be used for constitutive modeling purposes.

In the C3DHM model, 19 model parameters are required to simulate the unsaturated soil behavior. The shear strength parameters are already calibrated in the previous section (two parameters). Ten other parameters control the mechanical behavior, and the rest control the hydraulic and hysteresis behavior. In the below procedures, the stiffness parameters in the C3DHM model are calibrated from the CWOD test results considering the provided formulation for the K_0 coefficient, as follows:

1. Prepare the experimental data for each oedometer test (i.e., $(\sigma_1 - u_a)_i$, s_i, and measured specific volume v_{mi}).
2. Find the preconsolidation stress from Figure 6*a* for each test using Casagrande's method (*87*).
3. Assume arbitrary initial values for the model parameters.
4. Starting from the initial conditions where the vertical stresses are zero, assume a small increase in the vertical stress $d(\sigma_1 - u_a)$ and considering the corresponding suction for each test calculate the increase in lateral stress $d(\sigma_3 - u_a)$ using Equation 20 for K_0 in the elastic zone.
5. Update the stress state as follows:

$$(\sigma_1 - u_a)_{i+1} = (\sigma_1 - u_a)_i + d(\sigma_1 - u_a) \tag{22}$$

$$(\sigma_3 - u_a)_{i+1} = (\sigma_3 - u_a)_i + d(\sigma_3 - u_a) \tag{23}$$

$$p_{i+1} = \frac{(\sigma_1 - u_a)_{i+1} + 2(\sigma_3 - u_a)_{i+1}}{3} \tag{24}$$

$$q_{i+1} = (\sigma_1 - u_a)_{i+1} - (\sigma_3 - u_a)_{i+1} \tag{25}$$

$$dp = p_{i+1} - p_i \tag{26}$$

$$dq = q_{i+1} - q_i \tag{27}$$

6. Calculate the elastic specific volume using Equation 1 and the elastic water specific volume from Equation 3.
7. Use $(\sigma_1 - u_a)_{i+1}$ and $(\sigma_3 - u_a)_{i+1}$ as a new initial state, and repeat steps 4 through 6 until the preconsolidation stress is reached.
8. For the elastoplastic part (i.e., beyond the preconsolidation pressure and at any reloading or drying zone), assuming a small increase in the vertical stress $d(\sigma_1 - u_a)$, calculate the incremental change in lateral stress $d(\sigma_3 - u_a)$ using Equation 21.
9. Update the stress state using Equations 22 through 27.
10. Calculate the total specific volume using Equation 5 and the total specific water volume from Equation 4. It is worth noting that results from Equation 5 are exactly equal to that from Equation 2 when the soil state is on the elastoplastic surface.
11. Repeat steps 7 through 10 for the reloading and elastoplastic zones and steps 4 through 6 for the elastic zones to calculate the stress path for the entire K_0 loading conditions.
12. Repeat steps 1 through 11 for all the CWOD tests.
13. Calculate and sum the square of differences between the measured and predicted specific volumes, v, and differences between the measured and predicted water specific volumes, v_w.
14. Use the SOLVER add-in in Microsoft Excel to search the minimum of the difference between measured and predicted values by changing the model parameters (not including M, and k) based on Equation 28. The stop criterion is set to be that the variations between the current and previous iterations for each of the model parameters are less than 0.001.

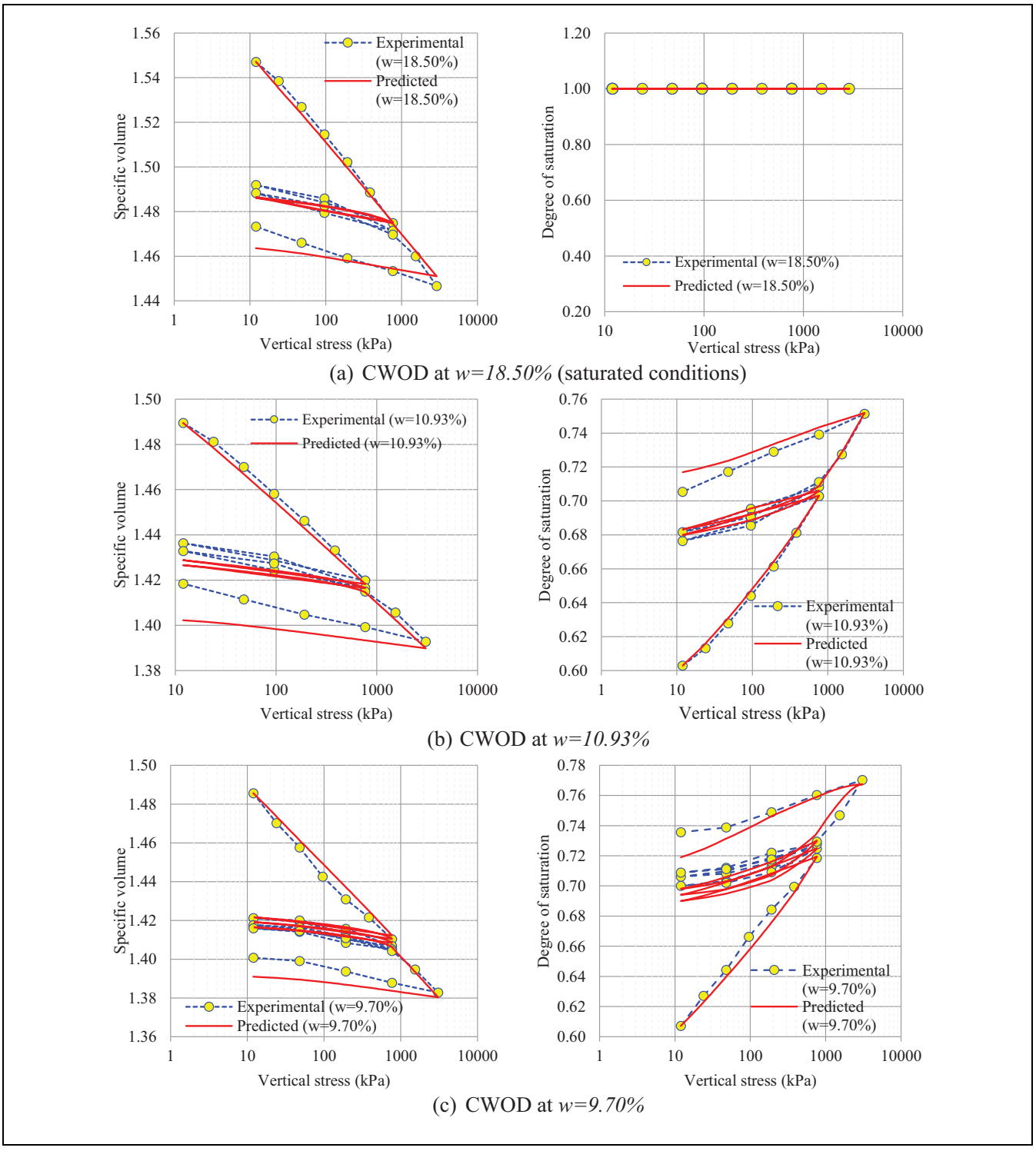

Figure 9. (continued)

$$F(X) = \sum_{i=1}^{n} w_i \left(v_{mi} - v_{pi}\right)^2 + \sum_{i=1}^{n} w_i \left(\left(v_w\right)_{mi} - \left(v_w\right)_{pi} \right)^2 \tag{28}$$

where subscripts "m" and "p" stand for measured and predicted, respectively.

Up to step 14, all the hydro-mechanical model parameters (including hysteresis) are calibrated. With this

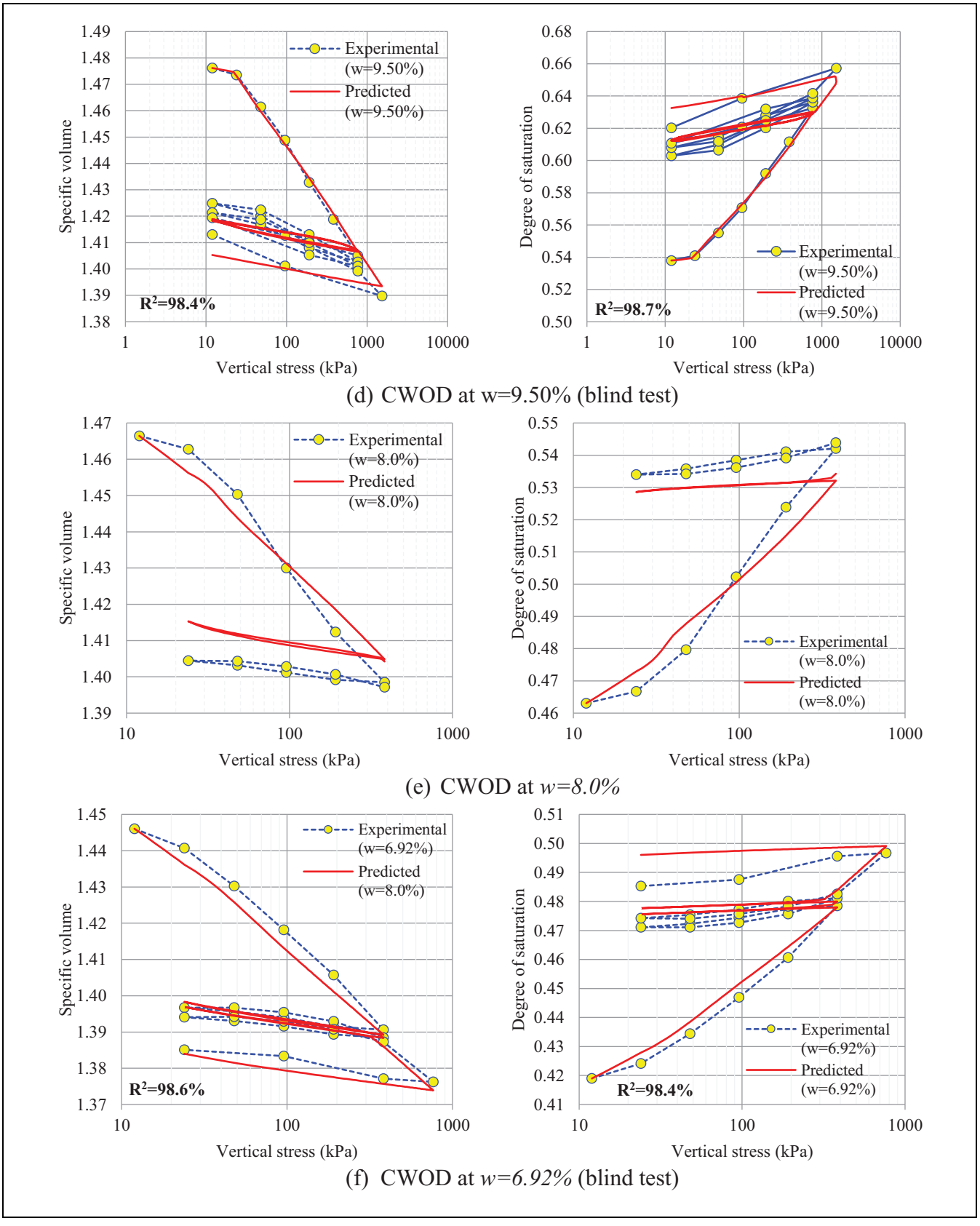

Figure 9. Comparisons of measured and predicted constant water content oedometer (CWOD) test results.

systematic procedure, provided in this section, we can take advantage of simple and fast tests (i.e., CWOD and CWDS) to calibrate all the model parameters.

Analysis Results and Discussion

The calibrated model parameters from four CWOD and nine CWDS tests are presented in Table 2. The elastic shear modulus can be calculated as follows: $G = 3(1 - 2\mu)(1 + e_0)p/(2\kappa(1 + \mu))$. Figure 9, *a–d*, compares the experimental results and predictions made by the C3DHM model using the calibrated parameters. Determination coefficients (R^2) of 98.0% and 98.1% were reached for v and S_r, respectively. This indicates strong correlations between the measured and predicted test results. Figure 9, *a–d*, also indicates that the predicted test results match the measured test results very well in elastic and elastoplastic zones.

The main objective of any constitutive model is to use limited test results to predict unlimited soil behavior under any arbitrary stress paths or loading conditions. Accordingly, two CWOD tests (at $w = 9.50\%$ and $w = 6.92\%$) were used as blind tests for validation purposes to examine how well the calibrated model parameters can predict the unknown soil behavior. The corresponding R^2 values were higher than 98% (as shown in Figure 9, *d* and *f*). Figure 9, *d* and *f*, also indicates that the predicted v and S_r values matched the measured test results very well for the whole of the stress paths. Results showed that the C3DHM model was able to capture the soil behavior under saturated and unsaturated conditions in a consistent manner. This is obvious from matching the soil behavior under saturated and unsaturated conditions at $w = 18.5\%$ and other oedometer tests simultaneously.

It is usually preferred to include different types of soil tests during the parameter calibration assignment to fully characterize the soil behavior. In this paper, two test results are included in the calibration process: (a) CWDS test and (b) cyclic CWOD. These two tests cover stiffness and strength behavioral features related to unsaturated soils. Moreover, constant water content testing of the soils provides the better representation for the coupling between hydraulic and mechanical behaviors. In other words, the C3DHM model was able to reasonably capture the elastoplastic hydro-mechanical behavior under cyclic anisotropic loading conditions. However, deviations were noticed in the cyclic loading–unloading zone. This can be attributed to the limited number of model parameters, intended to keep the model as simple as possible. Additional model parameters may be needed to overcome this limitation if higher accuracy is needed to model the coupled hydro-mechanical hystereses.

Concluding Remarks

In this research, conventional oedometer and direct shear devices were modified for unsaturated soils testing. The main modifications were to include a newly developed HST to measure suction changes during the CWOD and CWDS tests. In the CWOD tests, the volume change was measured by a digital indicator, and suction changes were monitored with the HST. In the CWDS tests, the vertical and lateral displacements were measured by LVDTs, and suction changes were monitored by means of a miniature HST. All the measurements were automatically recorded using a data logger. These minor modifications, in conventional testing devices, allowed for rapid testing of the hydro-mechanical behavior of unsaturated soils.

In addition, an elastoplastic hydro-mechanical model C3DHM as developed in Riad and Zhang (*74*) was used to fully characterize the soil behavior. The CWDS tests results were then used to calibrate the shear strength parameters in the model. Moreover, based on the K_0 formulation derived by Zhang et al. (*19*), the lateral stresses during CWOD were back-calculated. A procedure was then developed to calibrate the model parameters related to mechanical and hydraulic behaviors. Compacted silts were used to demonstrate the application of the proposed method. Results indicate that the proposed method and the C3DHM model were able to reasonably predict the soil behavior under cyclic undrained loading conditions. Moreover, the model was also able to predict the soil's behavior under saturated and unsaturated conditions. Some minor departures from observations were noticed during cyclic loading, which are attributed to the limited number of model parameters used (to keep the model as simple as possible). Additional model parameters may be needed to overcome this limitation if higher accuracy is needed to model the hysteresis behavior.

List of Notations

For equation notation, see Table 3.

Author Contributions

The authors confirm contribution to the paper as follows: study conception and design: Xiong Zhang and Beshoy Riad; data collection: Beshoy Riad; analysis and interpretation of results: Beshoy Riad and Xiong Zhang; draft manuscript preparation: Beshoy Riad, and Xiong Zhang. All authors reviewed the results and approved the final version of the manuscript.

Declaration of Conflicting Interests

The author(s) declared no potential conflicts of interest with respect to the research, authorship, and/or publication of this article.

Funding

The author(s) received no financial support for the research, authorship, and/or publication of this article.

ORCID iD

Beshoy Riad https://orcid.org/0000-0002-0215-915X

References

1. Briggs, K. M., F. A. Loveridge, and S. Glendinning. Failures in Transport Infrastructure Embankments. *Engineering Geology*, Vol. 219, 2017, pp. 107–117.
2. Skempton, A. W. Embankments and Cuttings on the Early Railways. In *The Civil Engineering of Canals and Railways before 1850* (Chrimes, M. M., ed.), Routledge, London, 2017, pp. 291–307.
3. Bishop, A. W., and I. B. Donald. The Experimental Study of Partly Saturated Soil in the Triaxial Apparatus. *Proc., 5th International Conference on Soil Mechanics and Foundation Engineering*, Paris, France, Dunod Press, Paris, 1961, pp. 13–21.
4. Bishop, A. W., I. Alpan, G. E. Blight, and I. B. Donald. Factors Controlling the Strength of Partly Saturated Cohesive Soils. *Proc., ASCE Research Conference on Shear Strength of Cohesive Soil*, Boulder, CO, 1960.
5. Thu, T. M., H. Rahardjo, and E. C. Leong. Soil-Water Characteristic Curve and Consolidation Behavior for a Compacted Silt. *Canadian Geotechnical Journal*, Vol. 44, No. 3, 2007, pp. 266–275.
6. Delage, P. Experimental Unsaturated Soil Mechanics. *Proc., 3rd International Conference on Unsaturated Soils*, Recife, Brazil, 2002, pp. 973–996.
7. Wheeler, S. J., and V. Sivakumar. Development and Application of a Critical State Model for Unsaturated Soil. *Proc., Wroth Memorial Symposium on Predictive Soil Mechanics*, St Catherine's College, Oxford, London, 1992.
8. Hoyos, L. R. Jr. *Experimental and Computational Modeling of Unsaturated Soil Behavior Under True Triaxial Stress States*. PhD dissertation. Georgia Institute of Technology, Atlanta, GA, 1998.
9. Sharma, R. S. *Mechanical Behaviour of Unsaturated Highly Expansive Clays*. PhD thesis. University of Oxford, Oxford, 1998.
10. De Campos, T. M. P., and C. W. Carrillo. Direct Shear Testing on an Unsaturated Soil From Rio de Janeiro. *Proc., 1st International Conference on Unsaturated Soils*, Paris, 1995, pp. 31–38.
11. Gan, J. K. M., D. G. Fredlund, and H. Rahardjo. Determination of the Shear Strength Parameters of an Unsaturated Soil Using the Direct Shear Test. *Canadian Geotechnical Journal*, Vol. 25, No. 3, 1988, pp. 500–510.
12. Gan, J. K. M., and D. G. Fredlund. Multistage Direct Shear Testing of Unsaturated Soils. *Geotechnical Testing Journal*, Vol. 11, No. 2, 1988, pp. 132–138.
13. Nam, S., M. Gutierrez, P. Diplas, and J. Petrie. Determination of the Shear Strength of Unsaturated Soils Using the Multistage Direct Shear Test. *Engineering Geology*, Vol. 122, No. 3, 2011, pp. 272–280.
14. Dineen, K., and J. B. Burland. A New Approach to Osmotically Controlled Oedometer Testing. *Proc., 1st International Conference on Unsaturated Soils*, Paris, 1995, pp. 459–465.
15. Hilf, J. W. *An Investigation of Pore Water Pressure in Compacted Cohesive Soils*. US Bureau of Reclamation, Denver, CO, 1956.
16. Kassiff, G., and A. B. Shalom. Experimental Relationship between Swell Pressure and Suction. *Géotechnique*, Vol. 21, No. 3, 1971, pp. 245–255.
17. Maswoswe, J. *Stress Paths for Compacted Soil During Collapse Due to Wetting*. PhD dissertation. Imperial College, London, 1985.
18. Romero, E., A. Lloret, and A. Gens. Development of a New Suction and Temperature Controlled Oedometer Cell. *Proc., 1st International Conference on Unsaturated Soils*, Paris, 1995, pp. 343–348.
19. Zhang, X., E. E. Alonso, and F. Casini. Explicit Formulation of At-Rest Coefficient and Its Role in Calibrating Elasto-Plastic Models for Unsaturated Soils. *Computers and Geotechnics*, Vol. 71, 2016, pp. 56–68.
20. Fredlund, D. G., and H. Rahardjo. *Soil Mechanics for Unsaturated Soils*. John Wiley & Sons, New York, NY, 1993.
21. Ridley, A. M., and J. B. Burland. A New Instrument for the Measurement of Soil Moisture Suction. *Géotechnique*, Vol. 43, No. 2, 1993, pp. 321–324.
22. Guan, Y., and D. G. Fredlund. Use of the Tensile Strength of Water for the Direct Measurement of High Soil Suction. *Canadian Geotechnical Journal*, Vol. 34, No. 4, 1997, pp. 604–614.
23. Li, L., and X. Zhang. Development of a New High-Suction Tensiometer. Geo-shanghai, Shanghai, China, 2014, pp. 416–425.
24. Lourenço, S. D. N., D. G. Toll, C. E. Augarde, D. Gallipoli, F. D. Evans, and G. M. Medero. Evaluation of Suction Measurement by the Tensiometer and the Axis Translation Technique. *Proc., 1st European Conference Unsaturated Soils Advances in Geo-Engineering, E-UNSAT*, Durham, UK, 2008, pp. 213–218.
25. Mancuso, C., and R. Papa. A High Capacity Tensiometer to Measure Soil Suction. *Proc., 20th IMEKO TC4 International Symposium: Measurement of Electrical Quantities*, Benevento, Italy, 2014, pp. 212–215.
26. Meilani, I., H. Rahardjo, E. C. Leong, and D. G. Fredlund. Mini Suction Probe for Matric Suction Measurements. *Canadian Geotechnical Journal*, Vol. 39, No. 6, 2002, pp. 1427–1432.
27. Rojas, J. C., L. Pagano, M. C. Zingariello, C. Mancuso, G. Giordano, and G. Passeggio. A New High Capacity Tensiometer: First Results. *Proc., 1st European Conference Unsaturated Soils Advances in Geo-Engineering, E-UNSAT*, Durham, UK, 2008, pp. 205–211.
28. Take, W. A., and M. D. Bolton. Tensiometer Saturation and the Reliable Measurement of Soil Suction. *Géotechnique*, Vol. 53, No. 2, 2003, pp. 159–172.
29. Tarantino, A., and L. Mongiovì. Design and Construction of a Tensiometer for Direct Measurement of Matric Suction. *Proc., 3rd International Conference on Unsaturated*

Soils, UNSAT2002, Recife, Brazil, Taylor & Francis, London, 2002, p. 319.
30. Toll, D. G., S. D. N. Lourenço, and J. Mendes. Advances in Suction Measurements Using High Suction Tensiometers. *Engineering Geology*, Vol. 165, 2013, pp. 29–37.
31. Li, Z. S., L. S. Tang, and J. M. Fleureau. Recent Developments and Applications of the High-Capacity Tensiometer in Geotechnical Engineering—A Review. *Electronic Journal of Geotechnical Engineering*, Vol. 22, No. 6, 2016, pp. 1805–1822.
32. Mendes, J., D. Gallipoli, A. Tarantino, and D. Toll. On the Development of an Ultra-High-Capacity Tensiometer Capable of Measuring Water Tensions to 7 MPa. *Géotechnique*, Vol. 69, No. 6, 2019, pp. 560–564.
33. Boso, M., E. Romero, and A. Tarantino. The Use of Different Suction Measurement Techniques to Determine Water Retention Curves. *Proc., Unsaturated Soils: Experimental Studies*, Springer, Berlin, Heidelberg, Germany 2005, pp. 169–181.
34. Cunningham, M. R. *The Mechanical Behaviour of a Reconstituted, Unsaturated Soil*. PhD thesis. Imperial College, London, 2000.
35. Lourenço, S. D. N., D. Gallipoli, D. G. Toll, C. E. Augarde, and F. D. Evans. A New Procedure for the Determination of Soil-Water Retention Curves by Continuous Drying Using High-Suction Tensiometers. *Canadian Geotechnical Journal*, Vol. 48, No. 2, 2011, pp. 327–335.
36. Toll, D. G., J. D. Asquith, A. Fraser, A. A. Hassan, G. Liu, S. D. N. LourenÓo, J. Mendes, T. Noguchi, P. Osinski, and R. Stirling. Tensiometer Techniques for Determining Soil Water Retention Curves. *Proc., 6th Asia-Pacific Conference on Unsaturated Soil*, Guilin, China, CRC Press/Balkema, Leiden, The Netherlands, 2015, pp. 15–22.
37. Marinho, F. A. M., and P. F. Teixeira. The Use of a High Capacity Tensiometer for Determining the Soil Water Retention Curve. *Soils & Rocks*, Vol. 32, No. 2, 2009, pp. 91–96.
38. Toker, N. K., J. T. Germaine, K. J. Sjoblom, and P. J. Culligan. A New Technique for Rapid Measurement of Continuous Soil Moisture Characteristic Curves. *Géotechnique*, Vol. 54, No. 3, 2004, pp. 179–186.
39. Lourenço, S. D. N., N. Jones, C. Morley, S. H. Doerr, and R. Bryant. Hysteresis in the Soil Water Retention of a Sand–Clay Mixture with Contact Angles Lower than Ninety Degrees. *Vadose Zone Journal*, Vol. 14, No. 7, 2015, p. vzj2014-07.
40. Li, L., X. Zhang, and P. Li. Evaluating a New Method for Simultaneous Measurement of Soil Water Retention and Shrinkage Curves. *Acta Geotechnica*, Vol. 14, 2019, p. 1021.
41. Li, L., and X. Zhang. Modified Unconfined Compression Testing System to Characterize Stress–Strain Behavior of Unsaturated Soils at Low Confining Stresses. *Transportation Research Record: Journal of the Transportation Research Board*, 2015. 2510: 54–64.
42. Ridley, A. M. Stress–Strain and Strength Relationships for a Reconstituted Clayey Silt. *Proc., 3rd International Conference on Unsaturated Soils, UNSAT 2002*, Recife, Brazil, CRC Press, Leiden, The Netherlands, 2002, p. 481.
43. Li, L., X. Zhang, and C. Lin. Development of an Oedometer Cell with Suction Measurement Ability. *Proc., Innovative Materials and Design for Sustainable Transportation Infrastructure*, Fairbanks, Alaska, 2015, pp. 179–188.
44. Li, L., and X. Zhang. A New Triaxial Testing System for Unsaturated Soil Characterization. *ASTM Geotechnical Testing Journal*, Vol. 38, No. 6, 2015, pp. 823–839.
45. Thu, T. M., H. Rahardjo, and E. C. Leong. Shear Strength and Pore-Water Pressure Characteristics during Constant Water Content Triaxial Tests. *Journal of Geotechnical and Geoenvironmental Engineering*, Vol. 132, No. 3, 2006, pp. 411–419.
46. Alonso, E. E., A. Gens, and A. Josa. A Constitutive Model for Partially Saturated Soils. *Géotechnique*, Vol. 40, No. 3, 1990, pp. 405–430.
47. Wheeler, S. J., and D. Karube. Constitutive Modelling. *Proc., 1st International Conference on Unsaturated Soils*, Paris, France, 1995.
48. Wheeler, S. J., and V. Sivakumar. An Elasto-Plastic Critical State Framework for Unsaturated Soil. *Géotechnique*, Vol. 45, No. 1, 1995, pp. 35–53.
49. Cui, Y. J., and P. Delage. Yeilding and Plastic Behaviour of an Unsaturated Compacted Silt. *Géotechnique*, Vol. 46, No. 2, 1996, pp. 291–311.
50. Wheeler, S. J. Inclusion of Specific Water Volume within an Elasto-Plastic Model for Unsaturated Soil. *Canadian Geotechnical Journal*, Vol. 33, No. 1, 1996, pp. 42–57.
51. Vaunat, J., E. Romero, and C. Jommi. An Elastoplastic Hydromechanical Model for Unsaturated Soils. *Experimental Evidence and Theoretical Approaches in Unsaturated Soils* (Tarantino, A., and C. Mancuso, eds.), CRC Press, Boca Raton, FL, Vol. 20, 2000.
52. Gens, A., M. Sánchez, and D. Sheng. On Constitutive Modelling of Unsaturated Soils. *Acta Geotechnica*, Vol. 1, No. 3, 2006, p. 137.
53. Gens, A. Soil-Environment Interactions in Geotechnical Engineering. *Géotechnique*, Vol. 60, No. 1, 2010, p. 3.
54. Jommi, C. Remarks on the Constitutive Modelling of Unsaturated Soils. *Experimental Evidence and Theoretical Approaches in Unsaturated Soils*, Vol. 153, 2000, pp. 139–153.
55. Zhang, X., L. Chen, and L. Li. Remarks on Constitutive Modeling of Unsaturated Soils. *Proc., Characterization, Modeling, and Performance of Geomaterials: Selected Papers From the 2009 GeoHunan International Conference*, Changsha, Hunan, China, 2009, pp. 13–19.
56. Wheeler, S. J., R. S. Sharma, and M. S. R. Buisson. Coupling of Hydraulic Hysteresis and Stress–Strain Behaviour in Unsaturated Soils. *Géotechnique*, Vol. 53, No. 1, 2004, pp. 41–54.
57. Gallipoli, D., A. Gens, R. Sharma, and J. Vaunat. An Elasto-Plastic Model for Unsaturated Soil Incorporating the Effects of Suction and Degree of Saturation on Mechanical Behaviour. *Géotechnique*, Vol. 53, No. 1, 2003, pp. 123–136.
58. Gallipoli, D., S. J. Wheeler, and M. Karstunen. Modelling the Variation of Degree of Saturation in a Deformable Unsaturated Soil. *Géotechnique*, Vol. 53, No. 1, 2003, pp. 105–112.
59. Sheng, D., S. W. Sloan, and A. Gens. A Constitutive Model for Unsaturated Soils: Thermomechanical and

Computational Aspects. *Computational Mechanics*, Vol. 33, No. 6, 2004, pp. 453–465.
60. Tamagnini, R. An Extended Cam-Clay Model for Unsaturated Soils with Hydraulic Hysteresis. *Géotechnique*, Vol. 54, No. 3, 2004, pp. 223–228.
61. Sun, D. A., H. B. Cui, H. Matsuoka, and D. C. Sheng. A Three-Dimensional Elastoplastic Model for Unsaturated Compacted Soils with Hydraulic Hysteresis. *Soils Found*, Vol. 47, No. 2, 2007, pp. 253–264.
62. Sun, D. A., D. C. Sheng, H. B. Cui, and S. W. Sloan. A Density-Dependent Elastoplastic Hydro-Mechanical Model for Unsaturated Compacted Soils. *International Journal for Numerical and Analytical Methods in Geomechanics*, Vol. 31, No. 11, 2007, pp. 1257–1279.
63. Sun, D., W. Sun, and L. Xiang. Effect of Degree of Saturation on Mechanical Behaviour of Unsaturated Soils and Its Elastoplastic Simulation. *Computers and Geotechnics*, Vol. 37, No. 5, 2010, pp. 678–688.
64. Mašin, D. Predicting the Dependency of a Degree of Saturation on Void Ratio and Suction Using Effective Stress Principle for Unsaturated Soils. *International Journal for Numerical and Analytical Methods in Geomechanics*, Vol. 34, No. 1, 2010, pp. 73–90.
65. Lloret-Cabot, M., M. Sánchez, and S. J. Wheeler. Formulation of a Three-Dimensional Constitutive Model for Unsaturated Soils Incorporating Mechanical-Water Retention Couplings. *International Journal for Numerical and Analytical Methods in Geomechanics*, Vol. 37, No. 17, 2013, pp. 3008–3035.
66. Raveendiraraj, A. *Coupling of Mechanical Behaviour and Water Retention Behaviour in Unsaturated Soils*. PhD thesis. University of Glasgow, Scotland, 2009.
67. Sheng, D., D. G. Fredlund, and A. Gens. A New Modelling Approach for Unsaturated Soils Using Independent Stress Variables. *Canadian Geotechnical Journal*, Vol. 45, No. 4, 2008, pp. 511–534.
68. Zhang, X., and R. L. Lytton. Discussion of: A New Modelling Approach for Unsaturated Soils Using Independent Stress Variables. *Canadian Geotechnical Journal*, Vol. 45, No. 12, 2008, pp. 1784–1787.
69. Zhang, X., and R. L. Lytton. Modified State-Surface Approach to the Study of Unsaturated Soil Behavior. Part I: Basic Concept. *Canadian Geotechnical Journal*, Vol. 46, No. 5, 2009, pp. 536–552.
70. Zhang, X., and R. L. Lytton. Modified State-Surface Approach to the Study of Unsaturated Soil Behavior. Part II: General Formulation. *Canadian Geotechnical Journal*, Vol. 46, No. 5, 2009, pp. 553–570.
71. Zhang, X., and R. L. Lytton. Modified State-Surface Approach to the Study of Unsaturated Soil Behavior. Part III: Modeling of Coupled Hydromechanical Effect. *Canadian Geotechnical Journal*, Vol. 49, No. 1, 2011, pp. 98–120.
72. Riad, B., and X. Zhang. Using Modified State Surface Approach to Study the Hydro-Mechanical Behavior of Unsaturated Soils. In *Geo-Congress 2020: Geo-Systems, Sustainability, Geoenvironmental Engineering, and Unsaturated Soil Mechanics* (Hambleton, J. P., R. Makhnenko, and A. S. Budge, eds.), American Society of Civil Engineers Geo-Congress 2020, Minneapolis, MN, 2020.
73. Riad, B., and X. Zhang. Modified State Surface Approach to Study Unsaturated Soil Hysteresis Behavior. *Transportation Research Record: Journal of the Transportation Research Board*, 2020. 2674: 484–498.
74. Riad, B., and X. Zhang. Consistent Three-Dimensional Elasto-Plastic Model to Study Unsaturated Soil Behavior with Considerations of Coupled Hydro-Mechanical Hysteresis. *Transportation Research Record: Journal of the Transportation Research Board*, 2021. 2675: 346–369.
75. Caruso, M., and A. Tarantino. A Shearbox for Testing Unsaturated Soils at Medium to High Degrees of Saturation. *Géotechnique*, Vol. 54, No. 4, 2004, pp. 281–284.
76. Lourenço, S. D. N., D. Gallipoli, D. G. Toll, and F. D. Evans. Development of a Commercial Tensiometer for Triaxial Testing of Unsaturated Soils. *Proc., 4th International Conference on Unsaturated Soils*, Phoenix, ASCE, Reston, VA, 2006, pp. 1875–1886.
77. Zhang, X., H. Lu, and L. Li. Use of Oedometer Equipped with High-Suction Tensiometer to Characterize Unsaturated Soils. *Transportation Research Record: Journal of the Transportation Research Board*, 2016. 2578: 58–71.
78. ASTM D1557. *Standard Test Methods for Laboratory Compaction Characteristics of Soil Using Modified Effort (56,000 ft-lbf/ft3 (2,700 kN-m/m3))*. American Society for Testing and Materials, West Conshohocken, PA, 2003.
79. Dafalias, Y. F., and E. P. Popov. A Model of Nonlinearly Hardening Materials for Complex Loading. *Acta Mechanica*, Vol. 21, No. 3, 1975, pp. 173–192.
80. Krieg, R. D. A Practical Two Surface Plasticity Theory. *Journal of Applied Mechanics*, Vol. 42, 1975, pp. 641–646.
81. Blight, G. E. Effective Stress Evaluation for Unsaturated Soils. *Journal of the Soil Mechanics and Foundations Division*, Vol. 93, No. 2, 1967, pp. 125–148.
82. Ho, D. Y. F., and D. G. Fredlund. Increase in Strength Due to Suction for Two Hong Kong Soils. *Proc., ASCE Specialty Conference on Engineering and Construction in Tropical and Residual Soils*, Hawaii, 1982, pp. 263–296.
83. Fredlund, D. G., N. R. Morgenstern, and R. A. Widger. The Shear Strength of Unsaturated Soils. *Canadian Geotechnical Journal*, Vol. 15, No. 3, 1978, pp. 313–321.
84. Wood, D. M. *Soil Behaviour and Critical State Soil Mechanics*. Cambridge University Press, New York, NY, 1990.
85. Li, S., B. Riad, X. Zhang, and Z. Liu. Characterization and Constitutive Modeling of Red Clay Contaminated with Ammonium Carbonate. *International Journal for Numerical and Analytical Methods in Geomechanics*, Vol. 44, No. 17, 2020, pp. 2329–2357.
86. Riad, B., and X. Zhang. Closed-Form Formulation for Continuous Prediction of At-Rest Coefficient for Saturated Soils. *International Journal of Geomechanics*, Vol. 19, No. 10, 2019, p. 4019110.
87. Casagrande, A. The Determination of Pre-consolidation Load and Its Practical Significance. *Proc., International Conference on Soil Mechanics and Foundation Engineering*, Cambridge, MA, 1936.